

# A Simple, Accurate Determination of Oxide PZC and the Strong Buffering Effect of Oxide Surfaces at Incipient Wetness

JAEHYEON PARK AND JOHN R. REGALBUTO<sup>1</sup>

*Department of Chemical Engineering, University of Illinois at Chicago, 810 South Clinton, Chicago, Illinois 60607*

Received January 30, 1995; accepted April 18, 1995

A special spear-tip semisolid electrode has been used to measure the pH of solid oxide–aqueous slurries at very high solid to liquid ratios. A simple non-Nernstian model of the oxide charging along with the experimental results demonstrate a very strong buffering effect of common oxide surfaces at high oxide content. This provides a simple, accurate measurement of oxide PZC which compares favorably to other common methods for PZC determination. The ramifications of the buffering effect on catalyst preparation are discussed. © 1995 Academic Press, Inc.

**Key Words:** point of zero charge (PZC or ZPC); isoelectric point (IEP); oxide; pH; electric double layer; proton adsorption; incipient wetness; dry impregnation.

## INTRODUCTION

The charging of solids suspended in aqueous solutions is an important factor in many physical phenomena such as colloid stability and ion adsorption. For nonelectrode materials such as clays and inorganic oxides, the traditional calculation of surface potential with the Nernst equation is not accurate (1–3). Healy and White have presented a number of more realistic yet simple “non-Nernstian” representations of oxide surfaces which assume a single type of chargeable hydroxyl group and employ the Gouy–Chapman model of the electric double layer (1, 2). The critical parameters of the model are the point of zero charge (PZC, that pH at which the net surface charge is zero), the difference between the two surface ionization constants  $K_1$  and  $K_2$ , often expressed as  $\Delta pK$  or  $DpK$  ( $= pK_2 - pK_1$ ), and the surface density of chargeable sites,  $N_s$  (OH groups/nm<sup>2</sup>). Perhaps the most important of these is the point of zero charge; in regard to catalyst preparation, the adsorption of cationic and anionic complexes can be qualitatively predicted based on this characteristic (4–7).

In solution, the hydroxyl groups at the surface of oxides become protonated and so positively charged at pH values below the oxide PZC, and deprotonated and so negatively charged above the PZC. The population or depopulation of protons to or from the surface as an oxide is added to a

liquid solution is reflected by pH changes in the bulk liquid. The coupling of the surface and bulk phases is elegantly demonstrated by the “mass titration” method of Schwarz, a simple method for finding an oxide’s PZC (8). In brief, as oxide is added to a liquid solution below (above) its PZC, the bulk pH increases (decreases) as the surface becomes protonated (deprotonated). With further additions of oxide the transfer of protons continues until the solution pH reaches the PZC, where there is no driving force for transfer. A drawback to this technique arises in the case of low surface area materials—at the very high mass of oxide needed to approach the oxide PZC, pH cannot be measured with a standard electrode.

The current work presents an extension of the modeling of surface charge and the measurement of oxide PZCs to solutions of high oxide mass percentage, at or close to the point of incipient wetness of the oxide (i.e., the amount of liquid added just equals the water-accessible pore volume of the solid). In these dense slurries liquid pH measurements are made with a spear-tip semisolid electrode. (The measurement of “equilibrium pH at high oxide loading,” will be abbreviated “EpHL.”) It will be shown that utilizing the condition of incipient wetness (highest possible mass content) provides a simple and accurate method to measure oxide PZCs which possesses advantages over other techniques such as the pH drift, acid–base potentiometric titrations, and even in some cases, mass titration. The model is absolutely necessary at the extremes of pH (<3 and >11), where the measured liquid pH does not correspond to the PZC even at high mass loadings.

The condition of high mass content, at or near the point of incipient wetness, is common for industrial methods of catalyst preparation. As the EpHL technique is demonstrated, the tremendous buffering capacity of oxide surfaces at high mass percentage can be fully appreciated. The ramifications on mechanistic interpretations of catalyst impregnation are discussed. The present oxide charging model has recently been included by the present group in a catalyst impregnation adsorption model (the adsorption of ionic metal complexes onto common oxide supports) (9). A companion paper to the present work involves the experimental procurement of  $DpK$  from the fitting of this single site charg-

<sup>1</sup> To whom correspondence should be addressed.

ing model to mass titration data and comprehensive modeling of surface charge for a number of common oxides (10).

### MATERIALS AND METHODS

A  $\gamma$ -alumina of surface area  $138 \text{ m}^2/\text{g}$  was used as received from LaRouche. Their  $\alpha$ -alumina was also used, but calcined at  $1050^\circ\text{C}$  for 4 h in a muffle furnace to reduce the surface area to  $30 \text{ m}^2/\text{g}$ . Ceria was prepared by calcining ammonium cerium (IV) nitrate (Aldrich) at  $800^\circ\text{C}$  for 6 h in the muffle furnace. Molybdena was prepared by calcining ammonium heptamolybdate (Aldrich) at  $500^\circ\text{C}$  for 5 h in the muffle furnace. The surface area of these two samples was 12 and  $1.8 \text{ m}^2/\text{g}$ , respectively. Cab-O-Sil fumed silicas L-90 and EH-5 were used as received, with surface areas of 100 and  $380 \text{ m}^2/\text{g}$ .

The oxide powders were wetted to incipient wetness. For example, 3.0 g of  $\gamma\text{-Al}_2\text{O}_3$  was placed into a 10-ml vial, and 2.5 ml of solution was required to reach the point at which the slurry surface became glossy when the vial was repeatedly tapped on the countertop. Distilled deionized water with a pH of about 5.7 was used. Solution pH was varied with  $\text{HNO}_3$  or  $\text{NaOH}$ , and  $\text{NaNO}_3$  was added to an ionic strength of 0.1 mol/liter. While there are obvious inaccuracies in assuming that bulk liquid pH measurement reflects solution pH in small pores, the electric double layer thickness (reciprocal Debye-Hückel parameter) at the ionic strength employed is  $9.6 \text{ \AA}$ , much less than the typical average pore radius of the oxides employed. From this standpoint, the majority of solution in pores can be considered as bulk liq-

uid, and will be in equilibrium with the external bulk solution provided long enough time is allowed for diffusive mixing. Results have shown that higher ionic strength speeds the approach to equilibrium, but does not in general change the final pH.

The pH of this thick slurry was measured with a spear-tip combination pH probe designed for food and other semisolid materials (Cole Parmer catalog number G-05988-20). Measurements were taken about 10 min after addition of the solutions. The pH meter was calibrated at pH values of 4 and 10 prior to each run. Comparison against a standard electrode revealed that pH measurement of the spear-tip electrode became somewhat inaccurate at the high pH extreme ( $>11$ – $12$ ). The reproducibility of day to day pH measurements, starting from independent calibrations, was  $\pm 0.15$  pH units. Multiple electrodes calibrated at the same time showed reproducibility usually greater than 0.1 pH unit. Electrode life was relatively short, often as little as a few weeks, as manifested by erratic readings and the failure to hold a calibration. The supplier confirmed that clogging of the reference junction was the likely cause.

Mass titrations were performed with various samples using a standard liquid filled combination electrode, to the limit of about 10 mass% of solid.

### THEORY

The non-Nernstian oxide charging model utilized here is a simple treatment of an amphoteric surface (1, 2, 11). The charging mechanism is expressed as

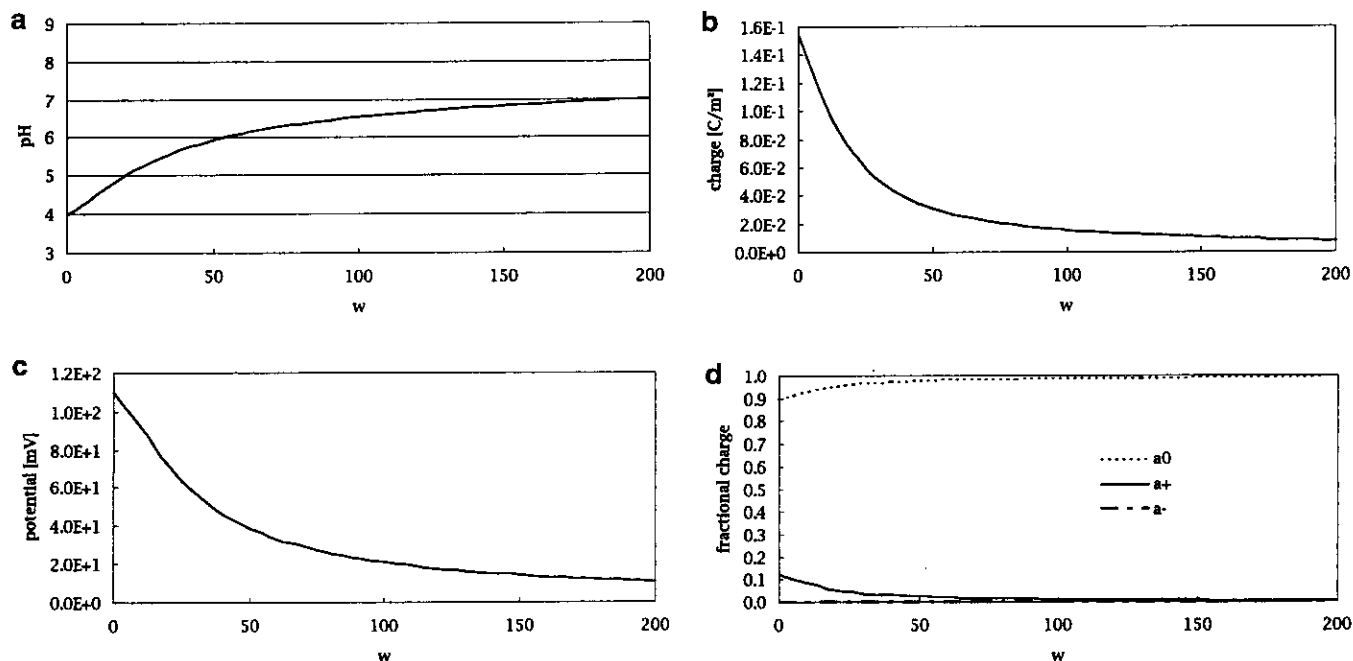


FIG. 1. Numerical simulation of mass titration ( $w = 200 \text{ g/liter}$ ,  $\text{PZC} = 8.0$ ,  $\text{Dp}K = 6.0$ ,  $s = 10 \text{ m}^2/\text{g}$ ). Weight loading versus (a) final pH, (b) surface charge ( $\sigma_0$ ), (c) surface potential ( $\psi_0$ ), and (d) fractional charge ( $a_0$  and  $a_+$ ).

$$[MOH_2^+] = \frac{K_1}{K_1 + [H_s^+]} [MOH] + [H_s^+] \quad [1]$$

$$[MOH] = \frac{K_2}{K_2 + [H_s^+]} [MO^-] + [H_s^+], \quad [2]$$

where  $[MOH_2^+]$ ,  $[MOH]$ , and  $[MO^-]$  represent the concentrations of positive, neutral, and negative surface groups on the solid, respectively, and  $[H_s^+]$  is the proton concentration at the oxide surface. The intrinsic acidity constants for protonation and deprotonation are written assuming the law of mass action:

$$K_1 = \frac{[MOH]}{[MOH_2^+]} [H_s^+] \quad [3]$$

$$K_2 = \frac{[MO^-]}{[MOH]} [H_s^+]. \quad [4]$$

A Boltzman distribution relates the surface to the bulk proton concentration

$$[H_s^+] = [H^+] \exp(-y_0), \quad [5]$$

where

$$y_0 = e\psi_0/kT,$$

$k$  is the Boltzman constant,

$T$  is absolute temperature,

$e$  is the electron charge ( $1.6 \times 10^{-19}$  C), and

$\psi_0$  is the surface potential.

The areal surface charge,  $\sigma_0$  (C/m<sup>2</sup>), expressed in terms of the charged groups is then

$$\begin{aligned} \frac{\sigma_0}{F\Gamma_t} &= \frac{[MOH_2^+] - [MO^-]}{[MOH_2^+] + [MOH] + [MO^-]} \\ &= a_+ - a_- \\ &= \frac{[H^+] \exp(-y_0)/K_1 - K_2 \exp(y_0)/[H^+]}{[H^+] \exp(-y_0)/K_1 + 1 + K_2 \exp(y_0)/[H^+]}, \quad [6] \end{aligned}$$

where

$a_+$  is the fraction of positively charged sites,

$a_-$  is the fraction of negatively charged sites,

$F$  is the Faraday constant ( $9.649 \times 10^4$  C/mole), and

$\Gamma_t$  is the density of charged sites (moles/m<sup>2</sup>)

$$= 10^{-5} N_s/6.02.$$

At the PZC ( $\sigma_0 = 0, a_+ = a_-$ ) this equation reduces to

$$pH_{PZC} (= PZC) = (pK_1 + pK_2)/2. \quad [7]$$

The acidity constants are equal pH differences from the PZC and are not independent ( $pK_1 = pH_{PZC} - 1/2DpK, pK_2 = pH_{PZC} + 1/2DpK$ ). The charging parameters are thus  $N_s$  and  $DpK$ . Values for the hydroxyl density  $N_s$  can be found by techniques such as isotopic exchange, infrared spectroscopy, chemical reaction, and acid-base titration (3), and values for  $DpK$  are found utilizing potentiometric titration data (11), and recently from mass titration data (10). The density of hydroxyl groups assumed in all simulations is 8 OH

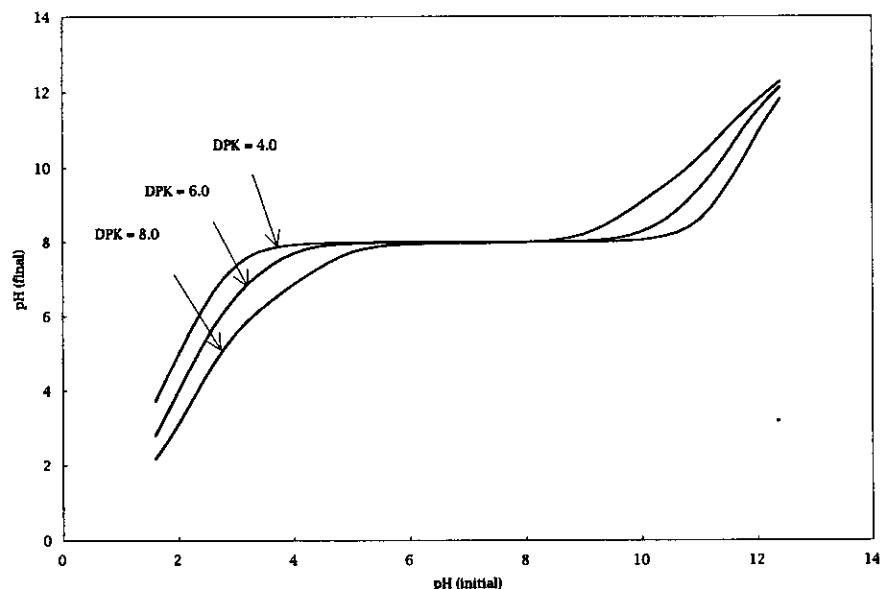


FIG. 2. EpHL simulation for various dpK values ( $w = 1000$  g/liter,  $PZC = 8.0$ ,  $DpK = 6.0$ ,  $s = 10$  m<sup>2</sup>/g).

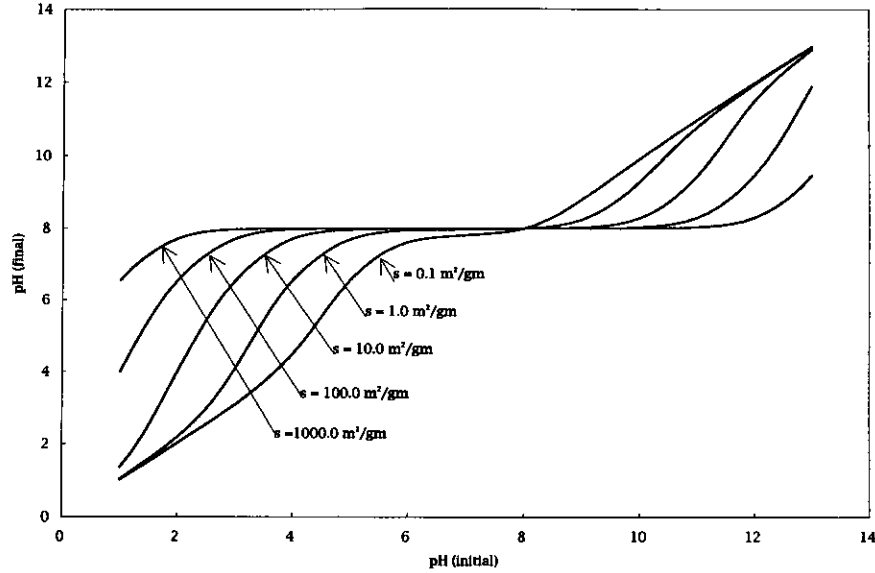


FIG. 3. EpHL simulation for various surface areas ( $w = 1000$  g/liter,  $PZC = 8.0$ ,  $DpK = 6.0$ ).

groups/nm<sup>2</sup> for alumina and 5 OH groups/nm<sup>2</sup> for silica, typical values for these oxides (3). The higher value is assumed for ceria and molybdena.

With the parameters supplied, Eq. [6] contains three unknowns,  $[H^+]$ ,  $\sigma_0$  (surface charge), and  $\psi_0$  (surface potential). Two additional equations are needed; the first is a relationship between charge and potential in the electric double layer. The relationship in the case of the Gouy–Chapman model is

$$\sigma_0 = (2\epsilon\epsilon_0kTn_0)^{1/2} \left[ \exp\left(\frac{ze\psi_0}{2kT}\right) - \exp\left(-\frac{ze\psi_0}{2kT}\right) \right], \quad [8]$$

where

$\epsilon$  is the relative dielectric constant of the solution,

$\epsilon_0$  is the permittivity of vacuum

( $8.854 \times 10^{-12}$  C<sup>2</sup>/Nm<sup>2</sup>), and

$n_0$  is the number of electrolyte ions per unit volume.

The second is a proton balance on the liquid phase, commonly used in acid–base potentiometric titration studies;

$$\sigma_0 = \frac{F}{ws} \left[ ([H^+]_0 - [OH^-]_0) + (10^{-(14-pH)} - 10^{-pH}) \frac{c^0}{y} \right], \quad [9]$$

where

$[H^+]_0$ ,  $[OH^-]_0$  are the initial concentrations of protons and hydroxyls,

$w$  is the mass concentration of oxide (g/liter),

$s$  is the specific surface area of the oxide (m<sup>2</sup>/g),

$y$  is the activity coefficient, from the extended

Debye–Huckel equation, and

$c^0$  is the standard concentration (1 mol/liter).

Once the charging parameters  $PZC$ ,  $N_s$ , and  $DpK$  are specified and the other physical constants and variables ( $w$ ,  $s$ ,  $[H^+]_0$ ,  $[OH^-]_0$ ) input, Eqs. [6]–[8] are solved simultaneously for  $[H^+]$ ,  $\sigma_0$ , and  $\psi_0$ . The model will now be applied to conditions of very high mass content.

## RESULTS AND DISCUSSION

The oxide charging model presented above has been considered sufficiently accurate for a qualitative explanation of physical trends (1, 3). It is used here first of all to compare the measurement of  $PZC$  at incipient wetness to other techniques, and to anticipate experimental results. Comparison with experiment then follows.

A simulated mass titration experiment is shown in Fig. 1. The parameters are a relatively low surface area (10 m<sup>2</sup>/g), a mid-range  $PZC$  (8.0), and a higher value of  $DpK$  (6.0). As the oxide mass increases, pH increases from the starting value of 4 (Fig. 1a). The surface charge and potential (Figs. 1b and 1c) are highest initially and decrease as oxide loading increases, since these quantities are normalized by the total

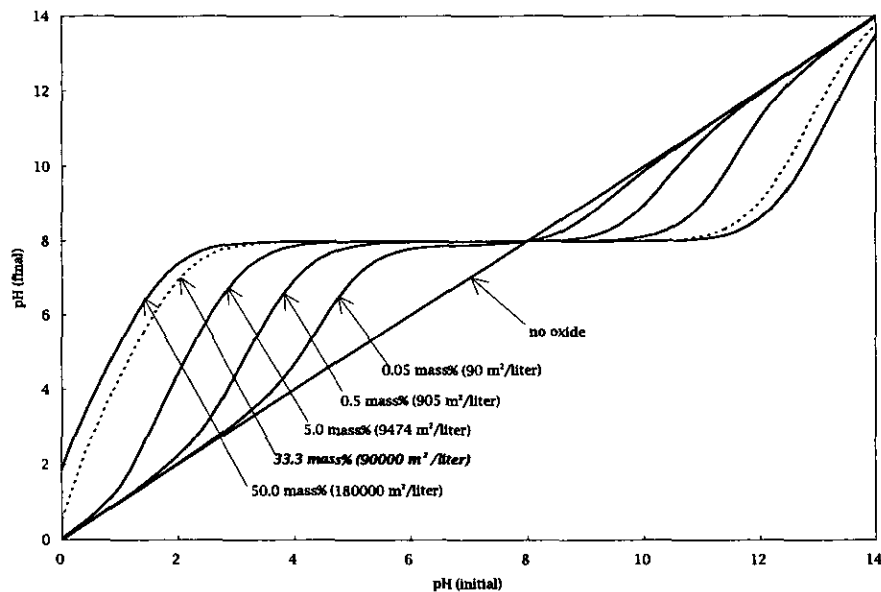


FIG. 4. Simulation of  $\gamma$ -alumina EpHL for various mass loadings (PZC = 8.0, DpK = 5.0,  $s = 180 \text{ m}^2/\text{g}$ ).

area of surface. In the limit of very high mass content the surface becomes neutrally charged; the number of protons which are removed from solution as pH rises is insignificant compared to the total number hydroxyl groups comprising the oxide surface. The fractions of positively and neutrally charged surface are shown in Fig. 1d. The fraction of neutrally charged surface,  $a_0 = [\text{MOH}] / \{[\text{MOH}_2^+] + [\text{MOH}] + [\text{MO}^-]\}$ , approaches unity at the PZC. The fraction of charged sites  $a_+$  and  $a_-$  becomes insignificant with respect to  $a_0$  near the PZC for DpK values greater than about 3 (1).

With the set of parameters chosen for Fig. 1, the final pH asymptote is not well developed at a mass loading of 200 g/liter. This limit is typical of mass titrations of common

oxides performed with standard pH electrodes. The experimental plateau misses the PZC by 1 pH unit. The advantage of utilizing a higher mass content will now be illustrated.

In Fig. 2, calculations are shown for the same simulated oxide (DpK = 8.0 and 4.0 also included) but at a weight loading, 1000 g/liter, which is typical of incipient wetness. The results are presented as final pH versus initial pH. In this format, each point represents the endpoint of a mass titration which would occur at 1000 g/liter. The plot reveals a wide plateau which corresponds to the PZC, and the position of this plateau is independent of the value of DpK. The measurement of equilibrium pH at high oxide loading would then appear to possess the simplicity of mass titration, as it

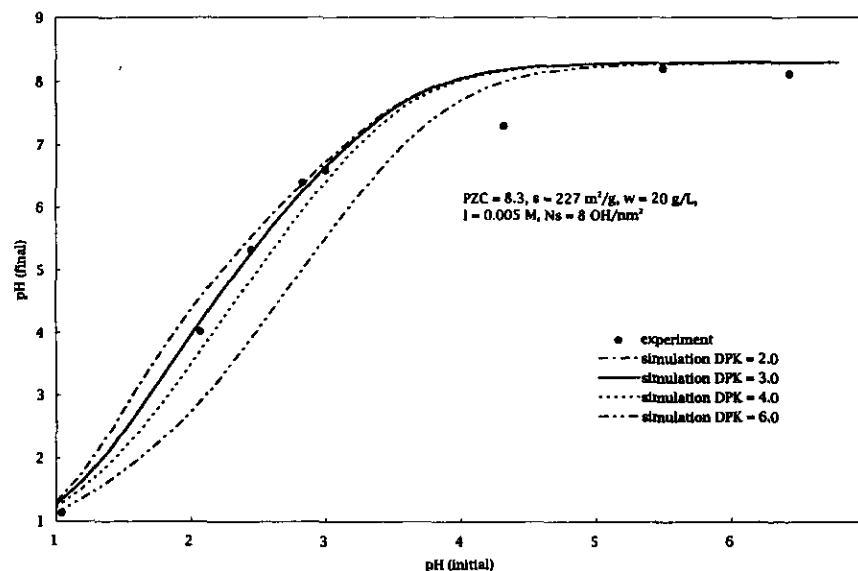


FIG. 5. Simulation of "equilibrium adsorption" experiment of Mang *et al.* (12) ( $w = 20 \text{ g/liter}$ , PZC = 8.3,  $s = 227 \text{ m}^2/\text{g}$ ,  $I = 0.005 \text{ mol/liter}$ ).

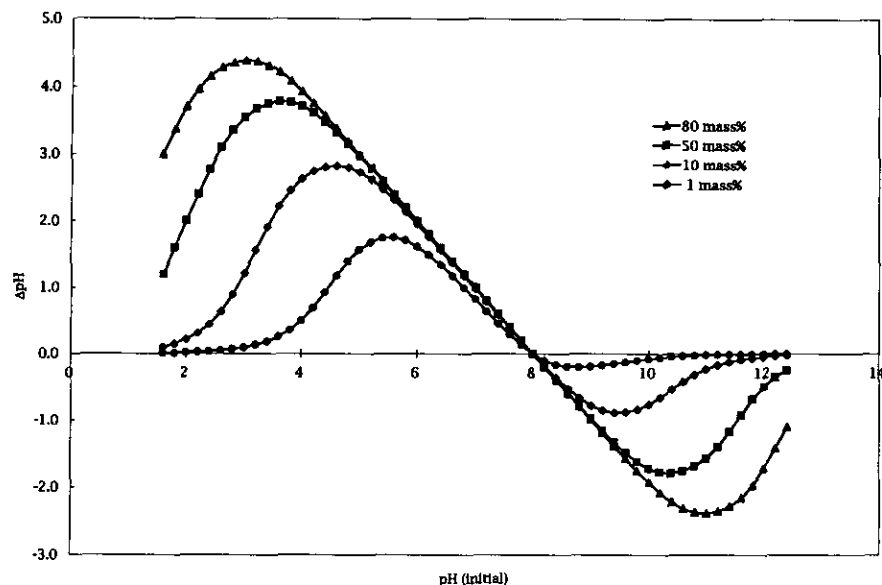


FIG. 6. EpHL simulation of Fig. 2 reformatted as  $\Delta\text{pH}$  versus  $\text{pH}$ .

consists only of making pH measurements of solid-liquid slurries. The technique possesses the advantage of working at the extremes of oxide loading where accuracy, as manifested in the width of the final pH plateau, is highest.

The plateau width is inversely proportional to  $\text{Dp}K$  (or a much weaker function of  $K_1$  and  $K_2$ ). As seen in light of Eqs. [3] and [4], at lower values of  $\text{Dp}K$  (smaller value of  $K_1$ , and larger value of  $K_2$ ) the oxide acts as a weaker acid or base, and with a higher propensity to remain neutrally charged it buffers the solution to a greater extent. Varying  $N_s$  or ionic strength has only a mild effect on the plateau width.

The sensitivity of the final pH-initial pH relationship to surface area is investigated in Fig. 3. Utilizing the same charging parameters ( $\text{Dp}K = 6.0$ ,  $\text{PZC} = 8.0$ ) and mass loading (1000 g/liter) as in Fig. 2, surface area is now varied over 5 orders of magnitude. The base case of Fig. 2 ( $\text{Dp}K = 6.0$ ) corresponds to the second curve from the bottom. A discernable plateau is seen even for the lowest surface area material,  $0.1 \text{ m}^2/\text{g}$ , although it is vertically displaced a bit from the  $\text{PZC}$ . The high sensitivity of the technique is due to the fact that proton transfer is a linear function of surface area (Eqs. [8] and [9]), but pH measurement is an exponential function. The middle of the pH scale is then "magnified" with respect to the pH extremes, permitting the observation of proton transfer even over small amounts of surface.

A second set of final versus initial pH curves is shown in Fig. 4 for a simulated oxide which corresponds to  $\gamma$ -alumina ( $\text{PZC} = 8.0$ ,  $s = 180 \text{ m}^2/\text{g}$ ,  $N_s = 8 \text{ OH}/\text{nm}^2$ ,  $\text{Dp}K = 5.0$ ). The mass percentage is varied from 50% or 1000 g/liter,

which approximates incipient wetness, down through three orders of magnitude. In fact, since mass concentration and surface area are multiplicative in Eq. [9], the series of curves can also represent a constant mass of oxide with varying surface area, as in the previous figure. The product of  $w$  and  $s$  might be termed "surface loading," with units  $\text{m}^2/\text{liter}$ , and is the most universal accounting of oxide addition. The surface loadings are included in the labels in Fig. 4.

The tremendous buffering power of alumina is seen in this figure; even at 0.05 mass% (a half gram of powder in a one liter vessel) pH can be attenuated by over 3 pH units in the central pH range. The value of 33 mass% corresponds to the industrial practice of 1:1 solution/support ratio in evaporator-type impregnations, assuming an average bed density of oxide pellets to be  $0.5 \text{ g}/\text{ml}$ . At 33 mass% the pH plateau is nearly as wide as that at incipient wetness, and begins dropping only below a pH of about 2. This result, verified by experiments shown below, has powerful ramifications with regard to catalyst preparation or any other process in which ionic complexes adsorb through a predominantly electrostatic mechanism (which is common (4-7)). That is, an extremely acidic or basic solution ( $\text{pH} < 1$ , or  $\text{pH} > 13$ ) is needed in order for the oxide surface to attain an appreciable charge. If only a weakly acidic or basic solution is employed, the final pH will be at the  $\text{PZC}$  of the oxide, and no electrostatic adsorption should occur.

The buffering effect of oxide supports has escaped consideration in the great majority of adsorption studies pertaining to catalyst impregnation. For example, in a recent experimental and modeling study of platinum adsorption on alu-

FIG. 7. Simulation of the pH drift experiment of Ahmed (13): (a) simulation and experimental data in  $\sigma_0$ - $\text{pH}_{\text{final}}$  format ( $\text{PZC} = 5.0$ ,  $\text{Dp}K = 8.0$  (fitted),  $s = 0.44 \text{ m}^2/\text{g}$ ,  $I = 0.1 \text{ mol}/\text{liter}$ ); (b) simulation in  $\Delta\text{pH}$  versus  $\text{pH}_{\text{initial}}$  format, 20 and 80 mass%; (c) simulation in  $\text{pH}_{\text{final}}$  versus  $\text{pH}_{\text{initial}}$  format, 20 and 80 mass%.

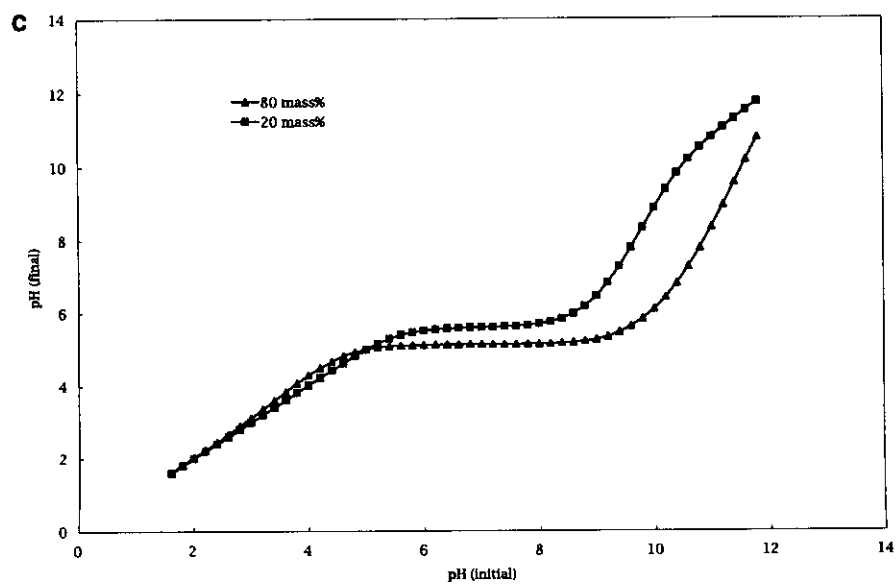
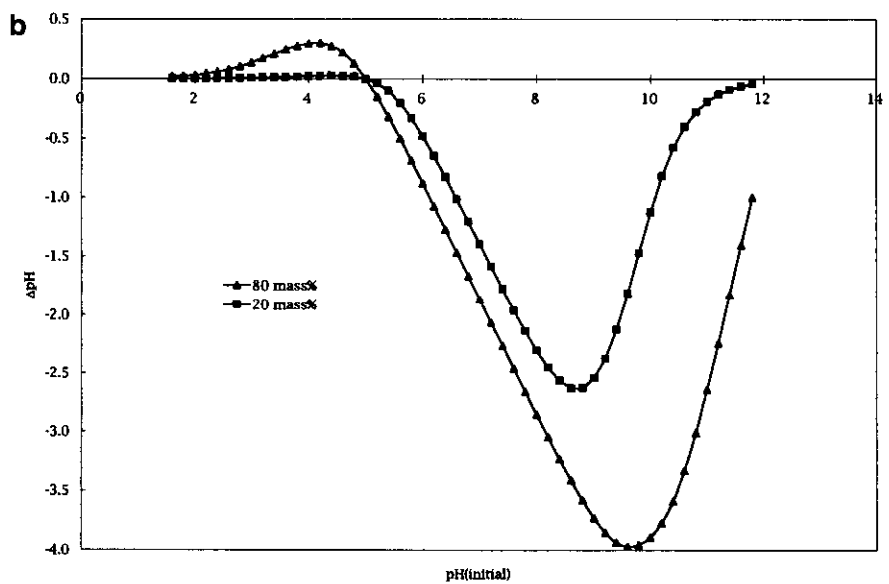
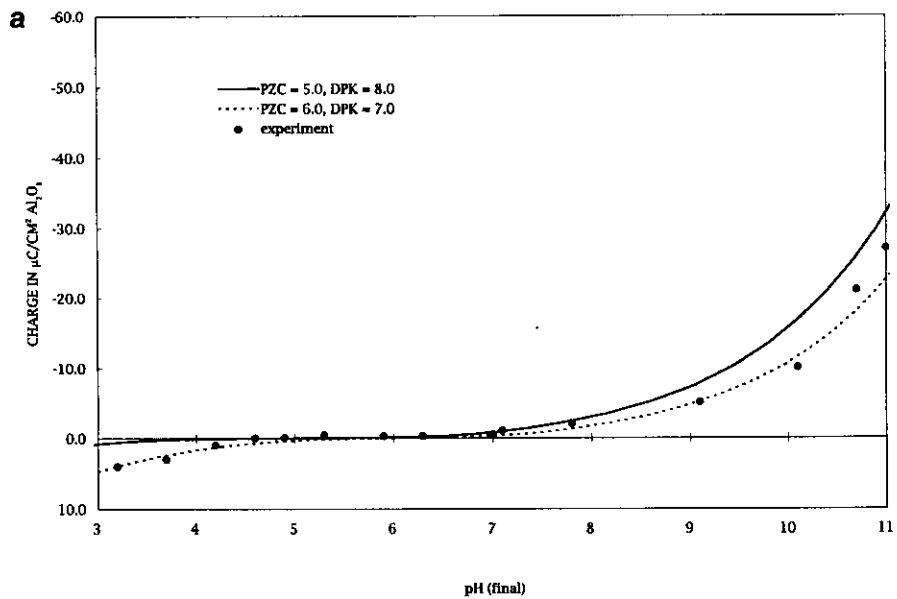


TABLE 1  
The Effect of PZC, DpK, and Surface Area on the Approach to PZC

	PZC	DpK	$s$ [m <sup>2</sup> /g]	$K_1$	$K_2$	$a_+$	$a_-$	$a_+/a_-$
Effect of PZC	7.0	4.0	100	10 <sup>-5</sup>	10 <sup>-9</sup>	9.8 × 10 <sup>-3</sup>	9.8 × 10 <sup>-3</sup>	1.00
	3.0	4.0	100	10 <sup>-1</sup>	10 <sup>-5</sup>	9.3 × 10 <sup>-3</sup>	1.0 × 10 <sup>-2</sup>	0.93
	2.0	4.0	100	10 <sup>0</sup>	10 <sup>-4</sup>	7.2 × 10 <sup>-3</sup>	1.3 × 10 <sup>-2</sup>	0.55
Effect of DpK	2.0	2.0	100	10 <sup>-1</sup>	10 <sup>-3</sup>	8.0 × 10 <sup>-2</sup>	8.7 × 10 <sup>-2</sup>	0.92
	2.0	4.0	100	10 <sup>0</sup>	10 <sup>-4</sup>	7.2 × 10 <sup>-3</sup>	1.3 × 10 <sup>-2</sup>	0.55
	2.0	6.0	100	10 <sup>1</sup>	10 <sup>-5</sup>	3.0 × 10 <sup>-4</sup>	3.3 × 10 <sup>-3</sup>	0.09
Effect of surface area	2.0	4.0	1000	10 <sup>0</sup>	10 <sup>-4</sup>	9.3 × 10 <sup>-3</sup>	1.0 × 10 <sup>-2</sup>	0.93
	2.0	4.0	100	10 <sup>0</sup>	10 <sup>-4</sup>	7.2 × 10 <sup>-3</sup>	1.3 × 10 <sup>-2</sup>	0.55
	2.0	4.0	10	10 <sup>0</sup>	10 <sup>-4</sup>	4.4 × 10 <sup>-3</sup>	2.2 × 10 <sup>-2</sup>	0.20

Note.  $N_s = 8 \text{ OH/nm}^2$ ,  $\text{pH}_0 = 9.0$ ,  $I = 0.1 \text{ M}$ , and  $w = 1000 \text{ g/liter}$ .

mina, large pH increases at high mass contents were attributed to ligand exchange reactions of metal complexes with the oxide surface which release hydroxyl groups to the liquid phase (12). A final pH versus initial pH simulation was made (Fig. 5) using their reported values of  $s$ ,  $w$ , and initial  $I$  ( $I$  was not constant but the effect of this variation is minor). The PZC was estimated from Table 1 in (12) to be 8.3. The simulated curves for various values of DpK all fall closely to the experimental data, which implies that the pH shifts can be explained solely on the basis of oxide buffering.

Noh and Schwarz have noted that mass titration is a variation of the pH drift method (8), and so is the present extended version of mass titration. In Fig. 6, the results of Fig. 2 have been reformatted as  $\Delta\text{pH}$  versus initial pH. Here the advantage of operating at high mass percentage is obvious, as a virtually straight line of high slope extends well beyond both sides of the  $x$  intercept at this condition.

Model results will now be compared to the pH drift measurements of Ahmed for a very low surface area alumina (13). This data was presented in the format of surface charge versus final pH (Fig. 1, (13)), also the format normally employed for potentiometric titrations. In Fig. 7a, the reported values of PZC (5.0), surface area (0.44 m<sup>2</sup>/g), mass loading (20%), and ionic strength (0.1 M) were used with a fitted value of DpK = 8.0 to reproduce the data reasonably well (solid line). The wide range in which the surface is neutrally charged (pH 4–8) makes the selection of an  $x$  intercept difficult. In fact, a PZC value of 6.0 fits the data even better, as shown by the dashed line. This same problem often arises in the determination of the common intersection point in potentiometric titrations.

Since surface charge is normalized by surface area, increasing the mass loading will have no effect on the shape of the curve in the surface charge–final pH format. An alternative format may be preferable, especially at high mass

loadings. A  $\Delta\text{pH}$  versus final pH format is shown in Fig. 7b, using the same parameters and with an additional simulation for 80 mass%. This higher mass loading value is typical for low surface area, low porosity materials at incipient wetness. A much clearer set of data would presumably appear at this condition, and utilize this format. The plateau-type final pH versus initial pH format (usual EpHL format) of both curves is shown in Fig. 7c. The same characteristic which incurs error in the surface charge– $\text{pH}_{\text{final}}$  plot (wide regime of neutral charge) actually enhances the accuracy of the PZC determination in the final pH versus initial pH format. It is noted that the 20 mass% calculation exhibits a plateau somewhat above the PZC, analogous to the lowest surface area employed in Fig. 3. At 80 mass%, the  $\text{pH}_{\text{final}}$  plateau does match the PZC. Reasons for the discrepancy at low mass loading (or surface area) are now discussed in conjunction with several other factors.

The deviations of the  $\text{pH}_{\text{final}}$  plateaus from the PZC seen in Figs. 3 and 7 can be explained by the extent to which the oxide surface is able to attain charge neutrality. At the PZC, by definition, the fraction of positively charged sites  $a_+$  equals the fraction of negatively charged sites  $a_-$  (Eq. [6]). Under some physical conditions, predominantly at the pH extremes, this is not achievable even at the maximum oxide loading (incipient wetness). Noh and Schwarz delineated a PZC range of 3–11 as that in which PZC determinations from mass titration were accurate (8), based on a pH measurement limitation of 10 mass% and typical values of charging parameters. A more detailed study of this limitation is shown in Fig. 8 and Table 1, in terms of the independent effects of PZC, DpK, and surface area,  $s$ . The parameters common to all plots are  $I = 0.1 \text{ M}$ ,  $N_s = 8 \text{ OH/nm}^2$ , and an oxide loading of 50 mass%.

In Fig. 8a (and top section of Table 1), the effect of PZC is investigated. With a DpK value of 4.0 and a surface area

FIG. 8. Analysis of plateau discrepancy at extreme parameter values: (a) effect of PZC; (b) effect of DpK; (c) effect of  $s$ .

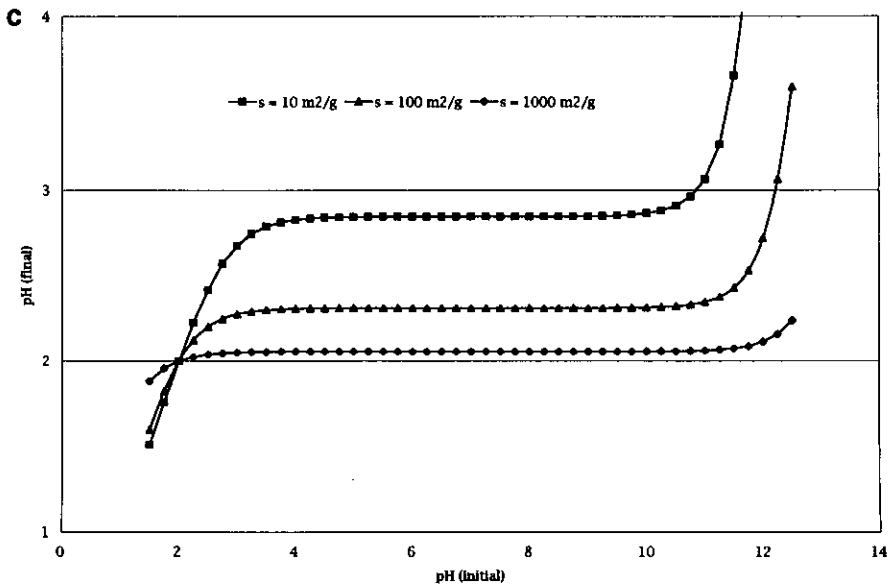
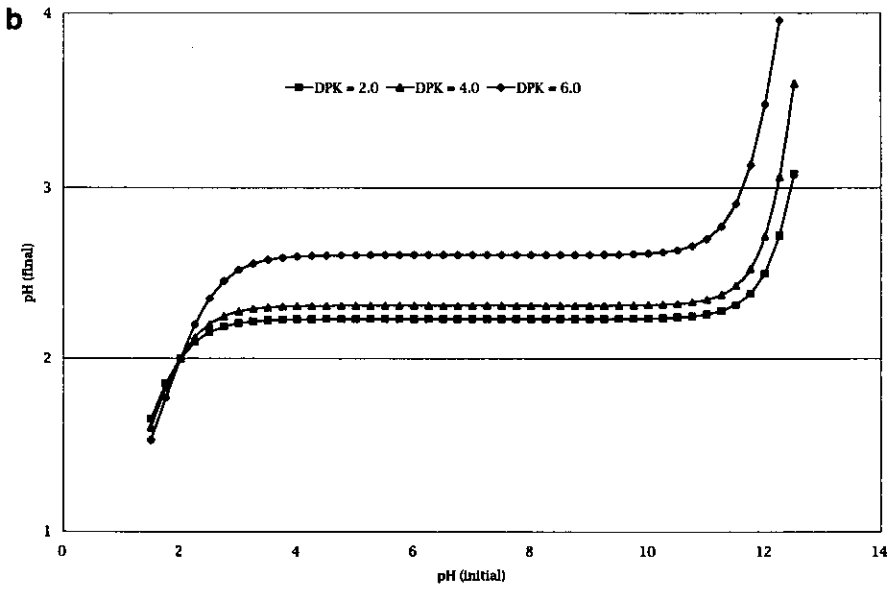
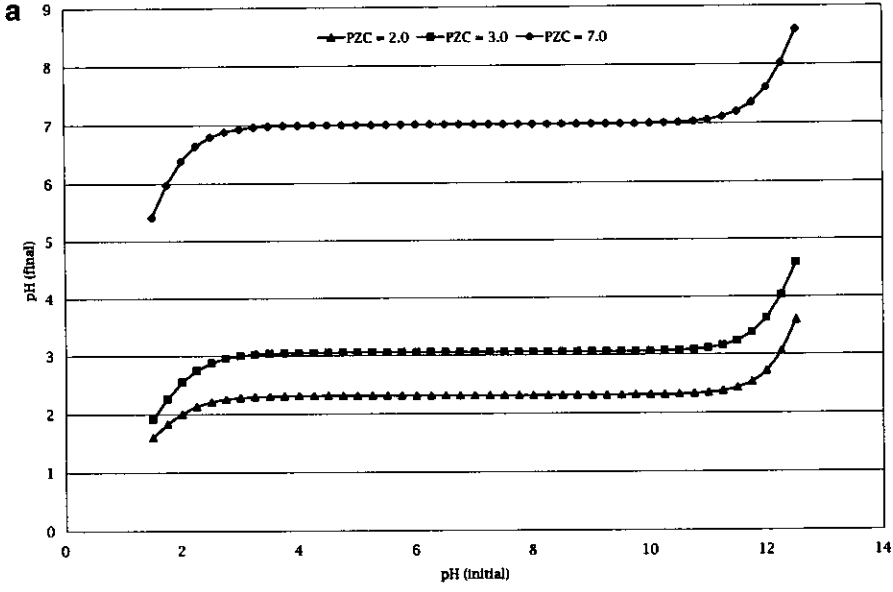


TABLE 2  
Characteristics of Oxide Samples and PZC Values by EpHL and Mass Titration and from the Literature

Sample	Specific surface area [m <sup>2</sup> /g]	Mass of sample/ volume of solution [g/ml]	Total oxide content %	PZC by mass titration	PZC by EpHL	PZC from references (8, 16-18)
$\alpha$ -Al <sub>2</sub> O <sub>3</sub>	30	1.0/2.5	28.6	8.5	8.3 ± 0.2	6.4 ~ 9.5
$\gamma$ -Al <sub>2</sub> O <sub>3</sub>	138	3.0/2.5	54.5	8.0	8.0 ± 0.2	6.9 ~ 9.5
CeO <sub>2</sub>	12	2.0/2.3	46.5	7.1	7.1 ± 0.2	6.75
SiO <sub>2</sub> (L-90)	100	1.0/2.5	28.6	<sup>a</sup>	3.4 ± 0.5	1.5 ~ 4.0
SiO <sub>2</sub> (EH-5)	380	1.0/2.3	30.3	<sup>a</sup>	3.0 ± 0.5	1.5 ~ 4.0
MoO <sub>3</sub>	1.8	4.0/1.0	80.0	<sup>a</sup>	-0.5 ± 1.0	1.50 ~ 6.25

<sup>a</sup> Could not be identified.

of 100 m<sup>2</sup>/g, the pH<sub>final</sub> plateau matches exactly the PZC for the PZC-7 sample, while the PZC-3 sample shows a small deviation, and the PZC-2 sample a significant one. As the value of PZC decreases, both acidity constants  $K_1$  and  $K_2$  increase, which causes  $a_+$  to decrease and  $a_-$  to increase (Eqs. [3] and [4]). The approach to charge neutrality can be expressed by the ratio of  $a_+$  to  $a_-$ , which should equal unity at the PZC. As the PZC decreases, the ratio  $a_+/a_-$  decreases. The  $a_+/a_-$  ratio is independent of pH<sub>initial</sub> at constant oxide loading. Thus, very low PZC samples do not reach their PZC even though the pH<sub>final</sub> curves exhibit a plateau.

Simulations for a material with PZC = 2 and a surface area of 100 m<sup>2</sup>/g are shown in Fig. 8b and the center section of Table 1. The deviation of the pH<sub>final</sub> plateau from the PZC increases as DpK increases. As DpK is increased, the value of  $K_1$  increases and the value of  $K_2$  decreases. However, the ratio of  $K_1$  to  $K_2$  increases with increasing DpK,

$$K_1/K_2 = 10^{\text{Dp}K},$$

which means that  $a_+$  decreases faster than  $a_-$  and again results in a smaller limiting value of ( $a_+/a_-$ ). In the central pH range (3 < pH < 11) this effect is usually not noticeable.

For a material with PZC = 2 and DpK = 4, the pH<sub>final</sub> plateau nearly corresponds with the PZC when the surface area is 1000 m<sup>2</sup>/g, but deviates significantly with decreasing surface area (Fig. 8c and Table 1, bottom section). This can be seen through a variation of Eq. [6] expressed in terms of the ratio ( $a_+/a_-$ ) and the surface proton concentration:

$$a_+/a_- = [H_s^+]^2/K_1K_2.$$

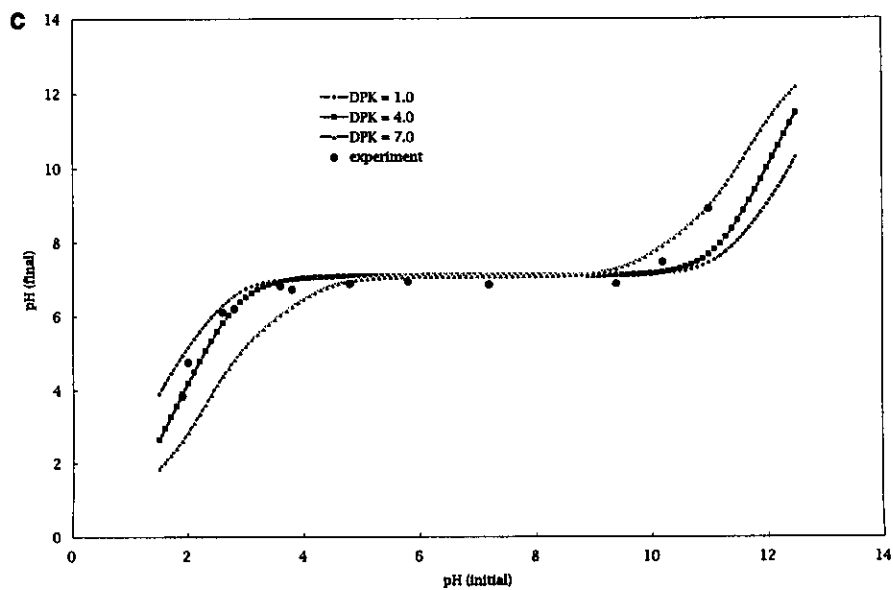
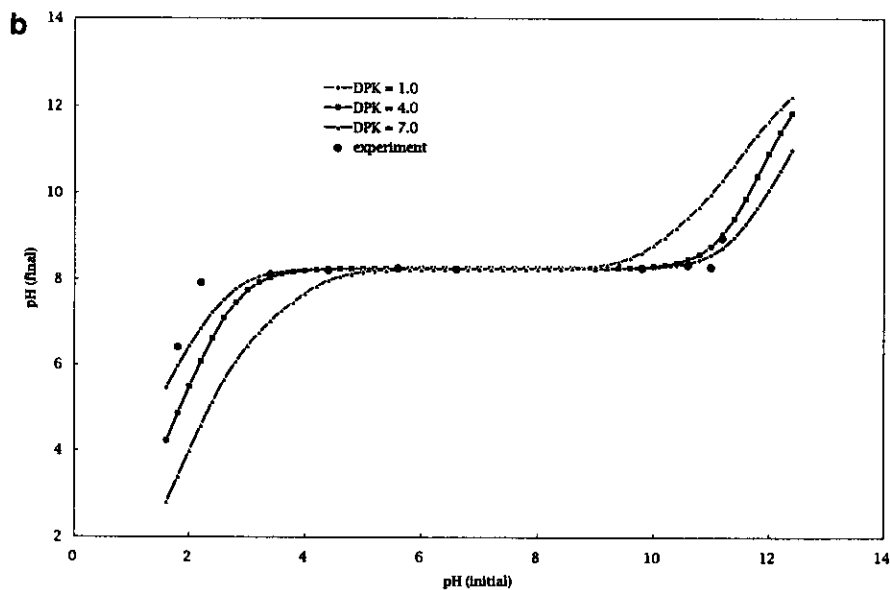
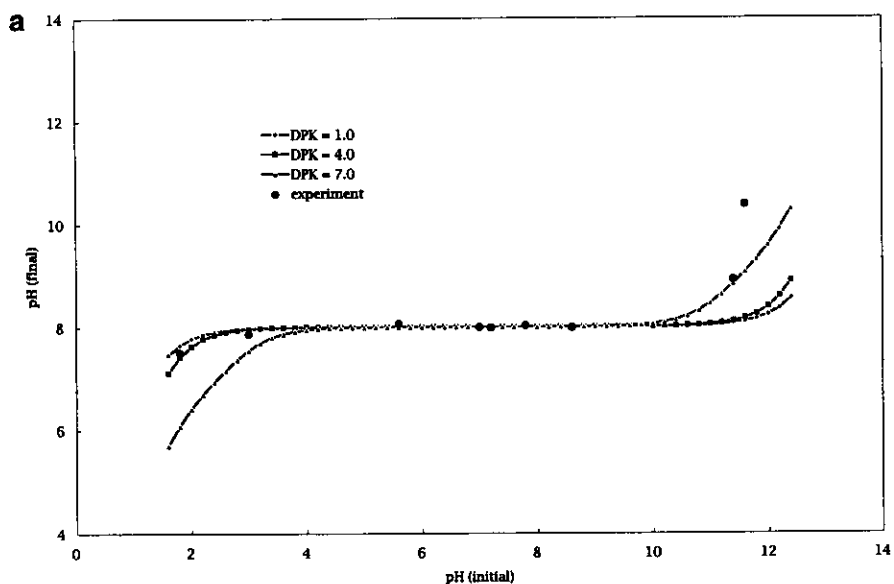
The denominator is fixed in this case. Higher surface area samples contain more protons per weight than the lower surface area materials, which supports a higher concentration of interfacial protons,  $[H_s^+]$ .

All three of the above effects are most predominant at the extreme PZC values, when  $K_1$  or  $K_2$  can become very large or small for moderate values of DpK. Deviations of the pH plateau from the PZC have the greatest sensitivity to PZC. For materials with a PZC above 7, the deviations of pH<sub>final</sub> plateau and PZC are opposite to those shown in Fig. 8, for analogous lines of reasoning. For example, the pH plateau of the low surface area sample is above the PZC in Fig. 7c, where the PZC is 5.0, while in Fig. 3 the pH plateau of the low surface area sample is below the PZC, since the PZC is 8.0.

A number of PZC determinations made by the present authors are shown in Figs. 9-11. The first set of materials exhibit mid-range PZC values and include a high surface area  $\gamma$ -alumina (138 m<sup>2</sup>/g, Fig. 9a), a low surface area  $\alpha$ -alumina (30 m<sup>2</sup>/g, Fig. 9b), and ceria (Fig. 9c) of surface area 12 m<sup>2</sup>/g. These materials were amenable to mass titration, and agreement between EpHL, mass titration, and literature values is good (Table 2). The error assigned to the EpHL measurements is that of the reproducibility of the electrode measurements, about ±0.2 pH unit.

Results for higher and lower surface area silica (380 and 100 m<sup>2</sup>/g) are shown in Fig. 10a and 10b, respectively. These materials possess higher surface area, but lower PZC values. Mass titration cannot be applied to silica with high certainty (8, 10). The PZC of silica has traditionally been difficult to measure by any technique, again due to the low slope of the  $\sigma_0$ -pH curve near the x-axis intercept (references 26 and 27 in (8)) and its low PZC. In Fig. 10a for silica EH-5, 380 m<sup>2</sup>/g and Fig. 10b for silica L-90, 100 m<sup>2</sup>/g, the simulated pH plateaus are a weak function of DpK, falling above the experimental plateaus at high values of DpK. Coincidence of the theoretical and experimental plateaus at the higher DpK values can be made by using a lower PZC value, thus the PZC cannot be determined uniquely from this data. With an independent determination of DpK the PZC can be better pinpointed. An optimization

FIG. 9. EpHL simulation and experimental results for: (a)  $\gamma$ -Al<sub>2</sub>O<sub>3</sub> ( $w = 1200$  g/liter, PZC = 8.0,  $s = 138$  m<sup>2</sup>/g); (b)  $\alpha$ -Al<sub>2</sub>O<sub>3</sub> ( $w = 400$  g/liter, PZC = 8.25,  $s = 30$  m<sup>2</sup>/g); (c) CeO<sub>2</sub> ( $w = 870$  g/liter, PZC = 7.1,  $s = 12$  m<sup>2</sup>/g).



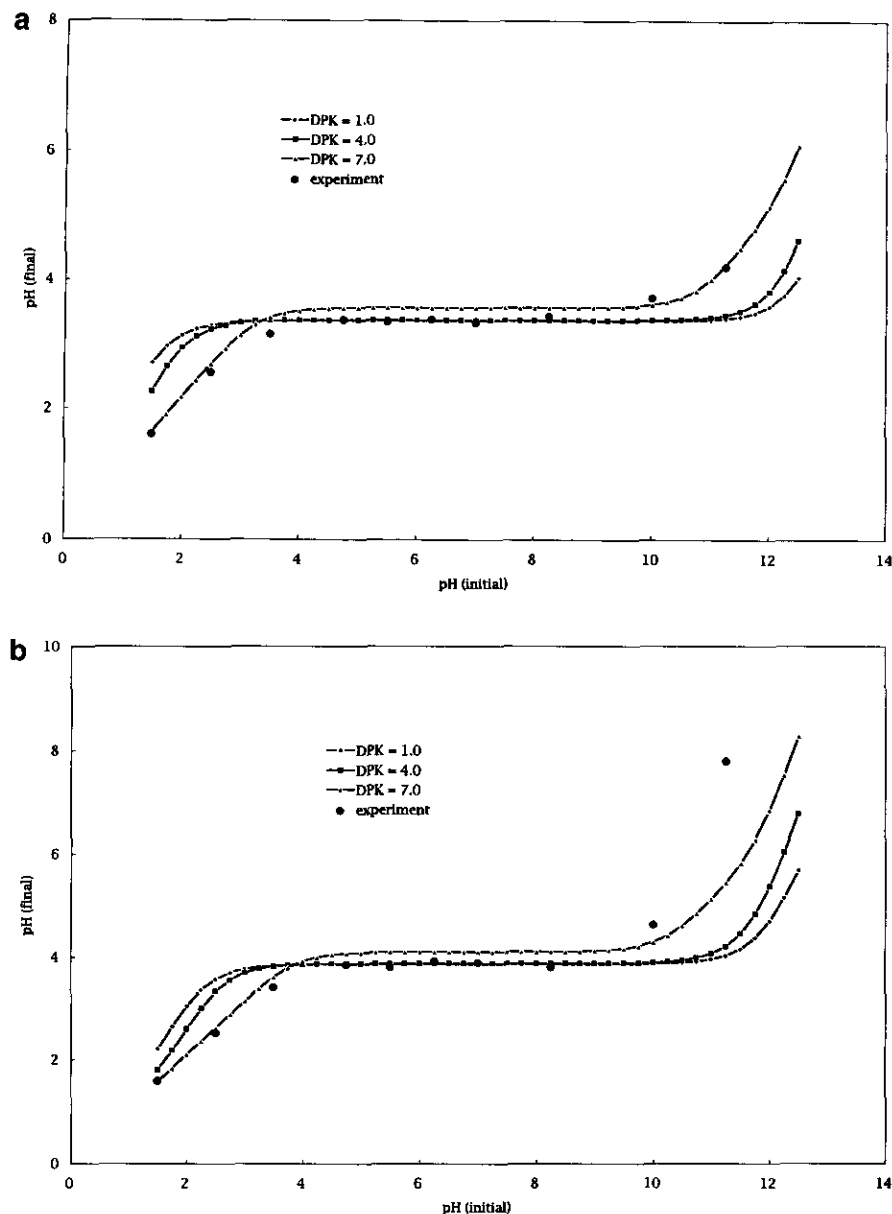


FIG. 10. EpHL simulation and experimental results for: (a) EH-5 SiO<sub>2</sub> ( $w = 435$  g/liter,  $s = 380$  m<sup>2</sup>/g); (b) L-90 SiO<sub>2</sub> ( $w = 400$  g/liter,  $s = 100$  m<sup>2</sup>/g).

of mass titration data fitting to obtain  $DpK$  values (10) suggests that the  $DpK$  values for these silicas are above 6, and that a good fit to the data can be achieved over a PZC range of about 0.5 unit. The best estimates of PZC for the EH-5 and L-90 silicas are  $3.0 \pm 0.5$  and  $3.4 \pm 0.5$ , respectively.

EpHL results are shown for molybdenum trioxide in Fig. 11. MoO<sub>3</sub> is hard to characterize material both for possessing a very low PZC, for having very low surface area (1.8 m<sup>2</sup>/g), and for its solubility above a pH of about 6. Due to these complications, literature results of its PZC are in conflict. An early attempt to measure the isoelectric point of MoO<sub>3</sub> by zeta potentiometry resulted in a value of 6.25 (14), and

was later reported by some of the same group by the same technique to be 2.9 (15). Parks' classic reference (16) gives a measured value of 1.5 for WO<sub>3</sub>, and assigns this value to metal trioxides in general. While a PZC of 4.0 for WO<sub>3</sub> was reported from mass titration (17), the same group in a subsequent paper presented this value as an estimate, since the low surface area of WO<sub>3</sub> made mass titration difficult (18).

With EpHL, the dissolution problem of MoO<sub>3</sub> is largely overcome owing to the relatively rapid approach to equilibrium; the solid spends only seconds in solutions at basic pH values. Typically for data points on the pH plateau, measured pH values were within one pH unit of the PZC in the several

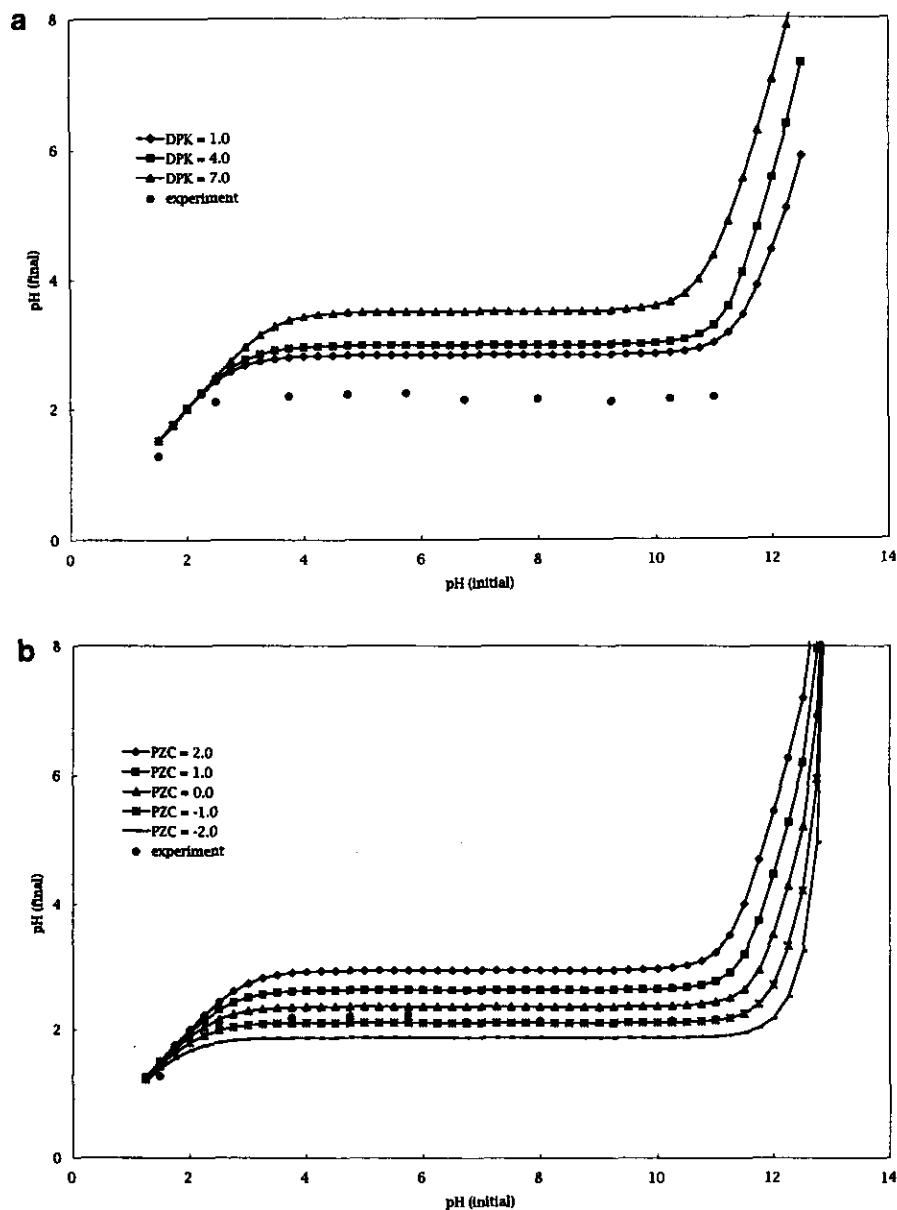


FIG. 11. EpHL simulation and experimental results for MoO<sub>3</sub> ( $w = 4000$  g/liter,  $s = 1.8$  m<sup>2</sup>/g): (a) variation of DpK at PZC = 2.1; (b) variation of PZC at DpK = 4.0.

seconds required to place the electrode into the just formed slurry. Thus MoO<sub>3</sub> was never subjected to basic solution more than for a few seconds, even at an initial solution pH of 11. The relative flatness of the data in the initial pH regimes below and above 6 confirms that dissolution can be neglected in these measurements.

EpHL results for MoO<sub>3</sub> exhibit a pH plateau at 2.1 (Fig. 11a). Attempts to simulate the pH plateau fail with a PZC of 2.1, however, at any value of DpK. The location of the plateau is now a strong function of DpK, but becomes weaker with low DpK. To find the best fit to the experimental data, several values of DpK were used for PZC values of 2.0, 1.0, 0, -1.0, and -2.0. The best fit, shown in Fig. 11b, is for a DpK value of 4.0 and a PZC of -1.0. Almost

as good a fit is obtained with a DpK of 1.0 and a PZC of 0.0. The slightly better fit and the higher value of DpK, which may be more typical of oxide surfaces, suggest that the former set of values is more realistic. The modeling error for the PZC for MoO<sub>3</sub> is the greatest for any sample, perhaps  $\pm 1.0$  pH unit. The value of the PZC for MoO<sub>3</sub> is estimated to be  $-0.5 \pm 1.0$  pH unit.

Thus the accuracy of the EpHL technique for PZC determination is high when PZC values are moderate, but diminishes as the extremes of pH are approached. Nonetheless, a relatively narrow range of values can be established at extreme pH. The applicability of the EpHL technique to low surface area samples is very useful, especially with moderate PZC materials. Its simplicity as compared to multitudinous

acid–base titrations of the common intersection point or pH drift techniques is also readily apparent. Accurate PZC measurements can be made with the present method for many samples with a few data points, spaced over a wide pH range. For high surface area materials such as  $\gamma$ -alumina, perhaps four pH measurements should be made in the range 3–11. No additional electrolytes are required for the present technique, the presence of which can result in specific adsorption and causes deviations of the common intersection point from the PZC. Solutions free of indifferent electrolytes are more representative of the actual solutions utilized in many processes such as catalyst impregnation. For low ionic strength solutions the slower approach of the pH measurement to equilibrium can be monitored visually using a chart recorder.

The disadvantages of this technique appear to be hardware related. Experience to date is that the electrodes have a service life of perhaps only several dozen or hundred measurements, likely from clogging of the reference junction. Measurement at very low pH may be a contributing factor. Standard or soil electrodes normally require an excess of solution, which would limit the accuracy of the present technique for the more difficult samples, but could be used in the mid-pH range for high surface area samples.

An indirect application of EpHL worth mentioning is the estimation of surface composition of mixed oxide materials. This analysis has been previously performed utilizing mass titration (17, 19) and electrophoresis (14, 15) data, but is difficult to perform when the oxide components have similar PZCs. With the increased sensitivity of EpHL the analysis of similar PZC mixed oxide systems may be more feasible.

Finally, while more elaborate models of oxide charging can be developed, as for example an approach based on a continuous proton affinity distribution (20), the present single site model of surface charging is thought sufficiently accurate to enable prediction of metal ion adsorption (9).

#### SUMMARY

A simple proton balance applied to high mass content slurries, in conjunction with a pH probe capable of measure-

ment at this condition, has fully revealed the strong buffering effect of oxide surfaces on solution pH. This effect occurs in many typical catalyst preparation processes, but is not usually accounted for. A simple, accurate measurement of oxide PZC has been developed based on the oxide buffering effect. The method can be easily applied and widely extended, even to materials possessing low surface areas and extreme PZC values.

#### ACKNOWLEDGMENTS

This project was initiated with NSF Award CBT8709019. The authors thank Professor Jim Schwarz for helpful discussions.

#### REFERENCES

1. Healy, T. W., and White, L. R., *Adv. Colloid Interface Sci.* **9**, 303 (1978).
2. Healy, T. W., *et al.*, *J. Electroanal. Chem.* **80**, 57 (1977).
3. James, R. O., and Parks, G. A., *Surf. Colloid Sci.* **12**, 119 (1982).
4. Brunelle, J. P., *Pure Appl. Chem.* **50**, 1211 (1978).
5. Anderson, J. R., "Structure of Metallic Catalysts." Academic Press, New York, 1975.
6. Schwarz, J. A., *Catal. Today* **15**, 395 (1992).
7. Wang, L., and Hall, K., *J. Catal.* **77**, 232 (1982).
8. Noh, J. S., and Schwarz, J. A., *J. Colloid Interface Sci.* **130**, 157 (1989).
9. Agashe, K., and Regalbuto, J. R., submitted for publication.
10. Park, J.-H., and Regalbuto, J. R., in preparation.
11. Noh, J. S., and Schwarz, J. A., *J. Colloid Interface Sci.* **139**, 139 (1990).
12. Mang, T., *et al.*, *Appl. Catal. A: Gen.* **106**, 239 (1993).
13. Ahmed, S. M., *J. Phys. Chem.* **73**, 3546 (1969).
14. Escudey-Castro, A. M., Broussieres McLeod, L., and Gil-Llambias, F. J., *Appl. Catal.* **4**, 371 (1982).
15. del Arco, M., *et al.*, *J. Catal.* **141**, 48 (1993).
16. Parks, G. A., *Chem. Rev.* **65**, 177 (1965).
17. Brady, R. L., *et al.*, *J. Catal.* **129**, 195 (1991).
18. Zhang, R., *et al.*, *J. Catal.* **138**, 55 (1992).
19. Subramanian, S., Noh, J. S., and Schwarz, J. A., *J. Catal.* **114**, 433 (1988).
20. Contescu, C., Jagiello, J., and Schwarz, J. A., *Langmuir* **9**, 1754 (1993).